REPORT

Contact person RISE
Michele Godio
Mathias Flansbjer
Natalie Williams Portal
Division Materials and Production
+46 10 516 50 94
michele.godio@ri.se

Date
2022-01-15

Reference

Optical strain measurement and crack detection technique for quasi-brittle masonry materials at high to ultra-high strain rates

RISE Research Institutes of Sweden AB
Chemistry and Applied Mechanics - Mechanical Research and Innovation

Performed by

Michele Godio
Mathias Flansbjer
Natalie Williams Portal

RISE Research Institutes of Sweden AB

Postal address
Box 857
501 15 BORÅS
SWEDEN

Office location
Brinellgatan 4
504 62 Borås
SWEDEN

Phone / Fax / E-mail
+46 10-516 50 00
+46 33-13 55 02
info@ri.se

Summary

Brick masonry is a construction material that has been widely used in Sweden in the XIX century, up to the first half of the XX century. As a result, masonry represents today a good portion of the Swedish built environment and is present in sensible targets such as monuments, churches, train stations and other strategically important buildings, which were not engineered to sustain the loads exerted by such extreme loading conditions. Assessing precisely the response and the level of damage reached by masonry during impacts and blasts is nonetheless very challenging. The present study investigates these intricated research questions by performing experimental tests to better characterize the response of URM walls against impacts. The walls were built by 'red' clay bricks and hydraulic lime-based mortar, a masonry typology that is found in many historic buildings in Sweden and, more generally, Northern Europe. The walls were tested at the laboratory of Applied Mechanics at RISE Research institutes of Sweden (Borås, Sweden). They were place into a test rig specifically designed for that purpose and subjected to dropping mass pendulum tests, in which they were repeatedly hit until the formation of heavily visible damage. The tests were instrumented with both hard-wired and optical measurements, these latter used along with high-speed (HS) cameras and Digital Image Correlation (DIC), to face the difficulty of observing cracks and determine strain measures at the time of the impact.

Keywords

Impacts | Masonry | Quasi-Brittle materials | Digital Image Correlation (DIC) | High-speed cameras | Crack detection | Strain-rate effects

Funding information

This study was funded by the ÅForsk Foundation, through the Young researcher granting scheme, grant agreement n. 20-335.

Table of contents

1. Introduction

Unreinforced masonry (URM) walls have a limited capacity towards impacts and explosions, particularly because of the weak tensile strength of the mortar and the brick-mortar interface. As such, the permissible deformation of the walls must be limited, which is particularly the case for loadbearing walls in buildings. Knowledge of loadbearing masonry walls' capacity to impacts and explosions is currently insufficient and therefore needs to be increased. Interest in this topic is rather scarce in the literature, as it has been growing in the last ten years only, see e.g. (Godio et al., 2021; Masi et al., 2019; Michaloudis and Gebbeken, 2019). This growing attention towards masonry structures finds its justification in the international socio-political context, where practitioners are increasingly demanded to assess the effect of impacts and explosions on civil structures (Masi et al., 2018).

Brick masonry is a construction material that has been widely used in Sweden in the XIX century, up to the first half of the XX century (Williams Portal et al., 2020). As a result, masonry represents today a good portion of the Swedish built environment and is present in sensible targets such as monuments, churches, train stations and other strategically important buildings, which were not engineered to sustain the loads exerted by such extreme loading conditions.

Assessing precisely the response and the level of damage reached by masonry during impacts and blasts is nonetheless very challenging. Masonry is a composite material made of bricks and mortar, whose quasi-brittle behaviour appears to be governed mainly by the properties of the mortar and the brick-mortar interface (Michaloudis and Gebbeken, 2019). Moreover, contrary to the static actions exerted by serviceability loads or settlements, or the dynamic actions generated by the wind or seismic events, which operate at relatively slow strain rates, the actions generated by impacts and blasts involve high to ultra-high strain-rates (Godio et al., 2021). It is known that, when high-rate strains occur, the material response, notably its stiffness and strength, change (Hao and Tarasov, 2008; Sielicki and Łodygowski, 2019). Unclear yet, is the way locally failure occurs, cracking initiates and develops, and strain waves propagate within the masonry at such high strain rates. Experimental tests are therefore needed to characterize the response, both at the material and structural level.

The present study investigates these intricated research questions by performing experimental tests to better characterize the response of URM walls against impacts. The walls were built by 'red' clay bricks and hydraulic lime-based mortar, a masonry typology that is found in many historic buildings in Sweden and, more generally, Northern Europe. The walls were tested at the laboratory of Applied Mechanics at RISE Research institutes of Sweden (Borås, Sweden). They were place into a test rig specifically designed for that purpose and subjected to dropping mass pendulum tests, in which they were repeatedly hit until the formation of heavily visible damage. The tests were instrumented with both hard-wired and optical measurements, these latter used along with high-speed cameras, to face the difficulty of observing cracks and determine strain measures at the time of the impact.

Pendulum-type tests are known to be optimal for brittle-fracture materials, as they can easily convey potential energy into impact energy. The literature on impact test on natural-scale masonry components is nonetheless very narrow, see e.g. (Gilbert et al., 2002). Investigated with the present tests is not only the overall response of the walls, but also the evidence of local failure, more particularly the crack initiation and propagation. A different axial load was applied on the top of the walls to study its effect on the cracking pattern, failure mechanism and number of repeated hits to open a breach into the wall. For this purpose the tests are instrumented with high-speed (HS) cameras and Digital Image Correlation (DIC).

Recent advances in imaging instrumentation, lighting resources, computational power and data storage capacity have brought optical measurements to cover a wide spectrum of applications across different fields of experimental mechanics (Jin et al., 2016). In this framework, the DIC is

a widely recognised method based on optical measurements, employing tracking and image-registration techniques to obtain very accurate measures of the 3D displacement and deformation field of a material (Sutton et al., 2009). Some of today's algorithms for the automated detection of cracks are based on results from the DIC (Cinar et al., 2017; Rezaie et al., 2021, 2020a, 2020b). Moreover, when used with high-speed cameras, the DIC method (or HS-DIC) becomes a relevant tool in the understanding of the deformation process and cracking of quasi-brittle materials at high- to ultra-high-rate strains. Yet, its use in this field is at its early stage, and limited to some construction materials like concrete (Flansbjer et al., 2018) and structural glass (Williams Portal et al., 2019).

In this study, the applicability of HS-DIC methods is proved on impact tests performed on full-scale brick masonry walls. Applications of the DIC method to masonry walls under impact conditions are, to the authors' knowledge, still unexplored. In fact, the use of DIC methods for masonry is limited to low-rate strains, that is for static (Bolhassani et al., 2017; Calderini et al., 2015; Ghorbani et al., 2015; Godio et al., 2019; Guerrero et al., 2014; Mojsilović and Salmanpour, 2016; Nabouch et al., 2019; Nghiem et al., 2015; Rezaie et al., 2019; Salmanpour et al., 2015; Shetty et al., 2019) and slow dynamic loads, like seismic and traffic loads (Acikgoz et al., 2018; Dhanasekar et al., 2019; Sieffert et al., 2016). In blast tests, high-speed cameras were used uniquely to observe the wall response during post-blast surveys, while deflections and strains were still measured by contact sensors like LVDTs and strain gauges (Godio et al., 2021). However, because sensors provide point-wise information of the state of deflection and strain of the walls, information on the local behaviour of the mortar and the brick-mortar interface is difficultly accessible by these means. In contrast, the emerging DIC techniques offer a versatile non-contact solution that allows the strain field and cracking to be determined over the entire range of points covered by the image. The study proves the applicability and validate the use of these methods in laboratory conditions, on tests made on structural components. Nonetheless, the experimental methodology developed here is general, as it can be applied to various test setups, loading conditions, and construction materials.

The paper is organized as follows. Section 2 describes the test units, while section 3 and section 4 focus on the test programme and test setup. Section 5 explains the instrumentation used and section 6 reports the main test results. Section 7 closes the paper.

2. Test units

Wall construction

Three URM walls were tested as part of the experimental programme (Figure 1). The walls had nominal height, width and thickness of about 1535 × 775 × 245 mm (Figure 2). They were built as part of a larger experimental campaign including the characterization of the static out-of-plane behaviour of unreinforced masonry (Williams Portal et al., 2022). In total 14 natural-scale walls were built, including single and double-wythe walls. Out of the double-wythe walls, 3 were tested against impacts. These walls are denoted as W9, W10 and W11. In all test units, reinforced concrete (RC) slabs were affixed below and over the brick walls to simulate the realistic contact conditions that can be found in existing buildings.

Bricks

The choice of the construction materials was motivated by the estimated construction time of loadbearing masonry walls in Sweden (pre-1940's). The walls were built using Swedish standard solid 'red' clay bricks with nominal dimensions of 250 × 120 × 62 mm. The actual dimensions were measured and appeared to be 245 × 115 × 62 mm. They were laid to form a regular pattern, with alternated stretchers and headers following a periodic Flemish-bond pattern, which required a skilled operator to build. The use of this specific brickwork, despite its name, appeared already in scattered areas of Northern and Central-East Europe on late medieval buildings.

Mortar

Both head (vertical) and bed (horizontal) joints were filled with hydraulic lime-based mortar of class D (CS I), with maximum aggregate size of ≤ 1 mm, and aggregate-to-binder ratio of 1:1 to 4:1 (Combimix's Hydrauliskt Kalkbruk, KKh). This mortar is used nowadays mainly for rendering purposes and is expected to have better mechanical properties and workability than the pure lime mortar that can be found in historic buildings. Hydraulic mortar is however more practical, because it can harden in both air and water and can nevertheless be used in humid environments as it is breathable (Skellefteå Museum, 2019). The joint thickness was maintained rather constant in the walls and around 10 to 12 mm.

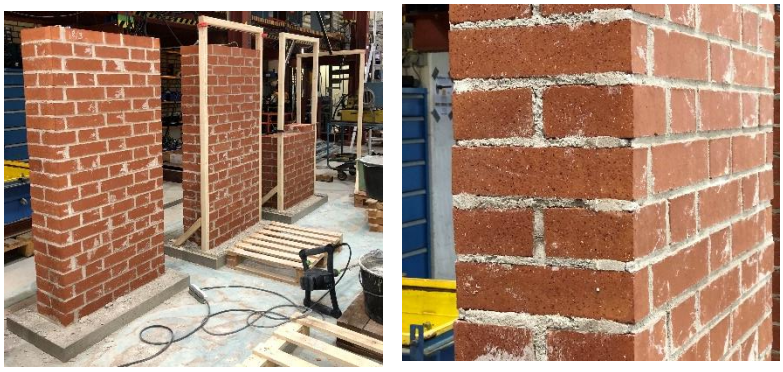

(a) (b)

Figure 1 Picture of the test units under construction (a); side view of the brickwork (b) .

Reinforce concrete slabs

Each wall was constructed between two reinforced concrete (RC) slabs of dimensions 980 × 500 × 75 mm (width × depth × height), see Figure 2. Concrete of the type C25/30 was used and two layers of steel reinforcement mesh were included in each slab. Four holes of diameter 22 mm were created at the corners of the top slabs, while four threaded lifting anchors (M12 NEO-BTK) were affixed in the corners of the bottom slabs. In this way, it was possible to lift and transport the test units by an overhead crane to the test setup without creating tensile stresses inside them.

Material properties

The walls were tested to impact 211 days after their construction. During the curing phase, the walls were left inside the laboratory, with smaller oscillations of temperature and humidity than the outdoor conditions. Characterization tests were carried out in parallel with the impact tests to derive the material properties of brick, mortar, and masonry as a composite material.

Bricks

The compressive strength f_c of the brick was determined according to EN 772-1: 2011 + A1: 2015 (EN 772-1, 2015). The bricks were reduced to prisms of dimensions 150 × 100 × 60 mm by the saw and their surface was prepared (sanded flat). The samples were then conditioned by drying them in a heating cabinet at 105 ± 5 ° C and allowed them to cool in climate room 20 ℃ and RF 50% 4 h before they were tested. Accordingly to (EN 772-1, 2015), the loading velocity was 0.6 MPa/s and a form factor of 0.75 was applied to the value obtained for the compressive strength. The density ρ of the bricks was determined following the specimen preparation.

The flexural tensile strength f_t of the bricks is not yet determined and will be obtained by subjecting brick prisms, carefully prepared and conditioned, to three-point bending.

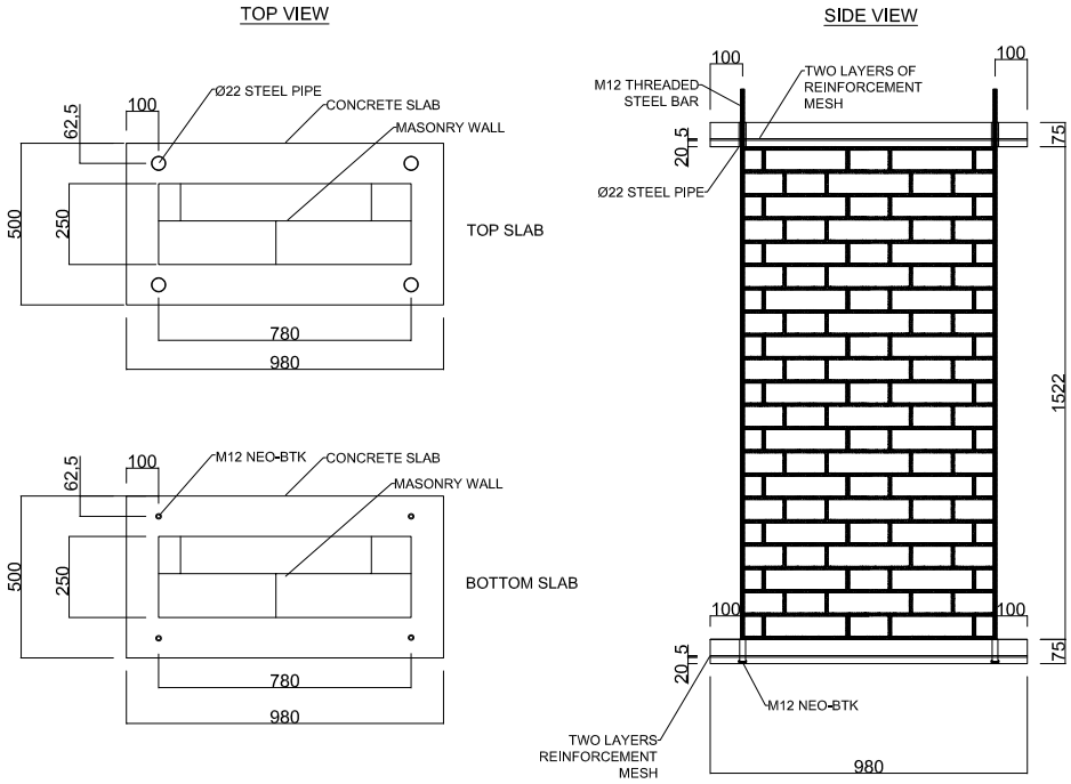

Figure 2 Geometry of the test units: (a) brick walls; (b) RC slabs.

Mortar

Tests for flexural and compressive strength of the mortar were performed 166-167 days after construction. The flexural tensile strength f_t of the mortar was measured following the EN 1015 (EN 1015-11, 2019) regulation, on prisms of dimensions 100 × 40 × 40 mm that were sampled when constructing the walls. The density ρ was also measured at the time of the flexural tensile tests. The compressive strength f_c of the mortar was measured according to EN 1015 (EN 1015-11, 2019) on the halves resulting from the flexural tensile tests. From the manufacturer, the mortar was reported to have a compressive strength of 0.4-2.5 MPa after 28 days.

Masonry

A double-wythe wallet of size 514 × 390 × 245 mm was built and subjected to an uniaxial compression test (EN 1052-1, 1992) about 200 days after construction. The axial force was applied at the speed of 1.0 mm/min at the top of the wallet by means of a loading plate fastened to a hydraulic actuator of 1 MN of capacity. Another steel platen was placed at the bottom of the wallet. From the analysis of the failure mechanism, which is not reported here for brevity, it appears that the wall was laterally confined during the test, as a consequence of the friction forces developing between the wallet and the steel plates.

Four unloading/reloading cycles were performed before reaching the peak force, at 0.5, 1.0, 1.5, 2.0 and 3.0 MPa. Then, the test was lead in monotonic way until failure of the axial loadbearing capacity of the wallet. Displacement field measurements were acquired by two 2D DIC measurement systems monitoring the front and back side of the specimen. Four virtual transducers measured the relative displacement over a base length that covered 2 units and 2 mortar layers. The compressive strength f_c was extracted by diving the maximum axial force by the wall cross section (EN 1052-1, 1992). The modulus of elasticity E was extracted as the secant modulus from the measure of the strain at all four measuring positions, at a stress equal to 1/3 of the maximum stress achieved (EN 1052-1, 1992). However, since initiation of cracking was observed for much

lower stress values (~1 MPa, i.e. about 1/8 of the maximum stress achieved), another method was used to derive *E*. This consisted in fitting the unloading/reloading cycles performed prior to reaching the peak force, observed by the 4 virtual transducers, and gave.

In addition to the uniaxial compression test, bond wrench tests will be conducted based on EN 1052-5 (EN 1052-5, 2005) on masonry couplets, to obtain an estimate of the flexural tensile strength of the masonry along the bed joints. The couplets will be held in a support bolted to a rigid table, while a clamp with lever arm will be applied to the top unit. The test will be instrumented with a load cell.

Table 1 Material properties resulting from the characterization tests.

Brick			**Mortar**			**Masonry**		
ρ **(kg/m^3)**	f_c **(MPa)**	f_t **(MPa)**	ρ **(kg/m^3)**	f_c **(MPa)**	f_t **(MPa)**	***E (MPa)***	f_c **(MPa)**	f_t **(MPa)**
1715 ± 4 (0.2 %; 6)	33.05 ± 0.69 (2.1 %; 6)	tbd	1570 ± 7 (0.5 %; 3)	0.85 ± 0.16 (18.3 %; 4)	0.38 ± 0.03 (7.7 %; 3)	2713 ± 564* (20.8 %; 4) 4865 ± 1289** (26,5 %; 20)	8.2 (0; 1)	tbd

Notation: mean ± standard deviation (C.o.V: coefficient of variation; number of samples tested).
* Value calculated according to EN 1052-1 (EN 1052-1, 1992)
** Value obtained by fitting unloading/reloading hysteresis cycles

Reinforced concrete

The RC used for the upper and lower slabs had compressive strength of 30 MPa, which was communicated by the producer.

3. Test programme

The experimental test programme consisted of 12 drop pendulum tests. The tests are listed in

Table 2 as they were chronologically executed. During the tests, the walls were subjected to repeated impacts until heavy damage was observed in the central part of the wall. We anticipate that none of the walls lost its axial loadbearing capacity during the test programme (see section 6 for more details). In fact, although damage was heavy, deformation was concentrated in the central part of the walls, thus not affecting their overall stability.

All the walls were tested under the same support conditions. The first series of tests were performed on wall W9 (test W9-1 up to test W9-5), which was used for exploratory tests on the definition of the impact mass and drop height to be used in the 2 successive specimens. Two different heights were initially applied, 0.5 and 1.0 m, with a dropping mass of 76.5 kg. The mass was later incremented to 116 kg and dropped from 1.0 m. This final configuration, i.e. 116 kg from 1.0 m, was used for the walls W10 and W11. These walls were repeatedly hit with the same mass-height configuration until the occurrence of heavy damage, which roughly corresponded to the opening of a breach in the wall (test W10-1 to W10-4, test W11-1 to W11-3). A different axial load was applied on the top of these two walls, respectively 0.2 and 0.05 MPa, to study its influence on the failure mechanism, crack propagation throughout the hits, and number of repeated hits needed to damage the wall heavily.

In one test (W10-4), technical issues with the lighting system prevented the 3D HS-DIC measurements to be recorded during the test. Still, a single set of pictures was taken at the end of that test, to be able to correlate the end status of the wall and compare it with the previous stages of the test (W10-1 to W10-3).

Table 2 Test programme.

Test	$H_w \times L_w \times t_w$ (mm)	Support condition - Stiffness (kN/mm)	Initial axial stress (MPa)*	Impact mass (kg)	Drop heigh (m)
W9-1	1535 × 775 × 245	Non rigid - 31.4	0.2	76.5	0.5
W9-2	“	“	“	“	1.0
W9-3	“	“	“	116.0	“
W9-4	“	“	“	“	“
W9-5	“	“	“	“	“
W10-1	1535 × 775 × 245	“	0.2	116.0	1.0
W10-2	“	“	“	“	“
W10-3	“	“	“	“	“
W10-4	“	“	“	“	“
W11-1	1535 × 780 × 245	“	0.05	116.0	1.0
W11-2	“	“	“	“	“
W11-3	“	“	“	“	“

* Value not including the self-weight of the steel platen and loading beam affixed to the top of the walls.

4. Test setup

The impact tests were conducted in a test rig simulating a drop rig for pendulum tests.

Test rig

Figure 3 shows the test rig in which the impact tests were conducted. The rig consisted in two steel frames of height 3.5 m and length 5.0 m. The frames were distanced by 1.2 m and mounted on a 220-mm thick steel floor which was, in turn, laid on the laboratory strong floor. The two frames were connected by a 200 × 200 mm HEB steel beam, reinforced by 4 flanges and placed transversally between the frames at 1.6 m from the steel floor (in brown in Figure 3).

The test units were assembled outside the test stand and were moved into it for testing by an overhead crane. In the stand, the lower RC slab was laid directly on the steel floor and pushed, by means of two threaded steel rods, against a 200 × 100 mm steel profile which ensured the force transfer between the slab and the base of the frame. The fixation system for the upper RC slab was designed to allow said slab to move vertically all while minimizing the friction and its rotation. The slab was pushed against the transversal beam and kept against it by a tie-down strap placed around the steel columns (in orange in Figure 3). Two Teflon sheets and an interposed layer of grease were placed between the upper slab and the transversal brown beam. A 50-mm thick steel loading platen was fastened to the top side of the upper RC slab; on the top of it, a 200 × 200 mm steel loading beam was fixed (in red in Figure 3). Finally, the axial force was applied through 2 lateral post-tensioned threaded M16 10.9 steel rods, connecting the loading beam directly to the steel floor. The rods were manually post-tensioned to the intended initial force before each drop.

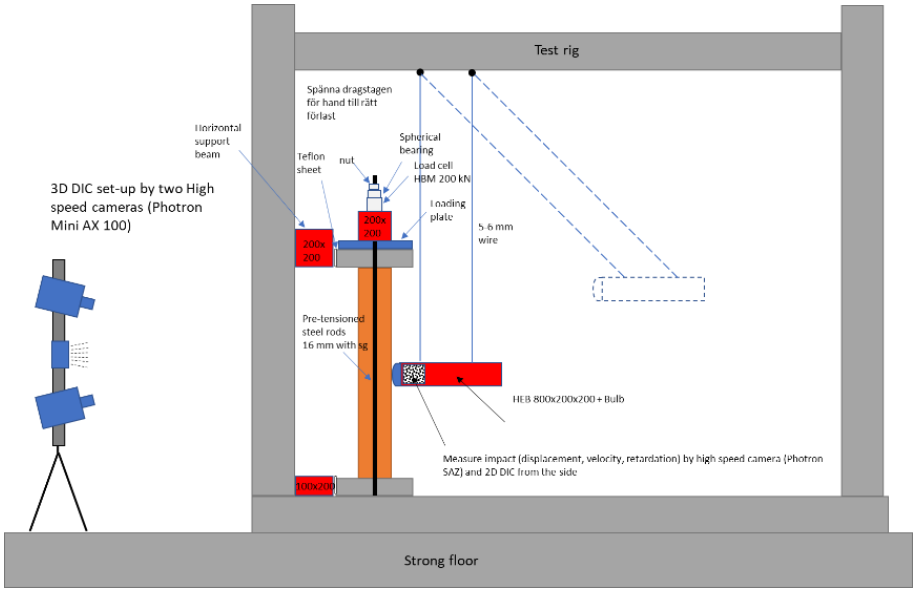

(a)

(b)

Figure 3 Test setup: schematic (a); bird-eye view taken before test W9-1 (b).

Dropping mass

A pendulum system was used to impact the brick walls. As impacting mass, we used a 800 × 200 × 200 steel HEB beam reinforced at its ends by two 15-mm thick steel flanges (Figure 4a). At the end of the beam impacting the walls, a steel plate with an attached steel bulb was screwed (Figure 4b). the bulb consisted of a steel cylinder with an hemispherical cap Figure 4b. In this basic configuration, the dropping mass weighted 76.5 kg. At the other end of the beam, a short steel beam was attached to reach the final configuration of 116 kg.

(a)

Figure 4 Dropping mass: lateral view.

Four cables connected the mass to the frame. The dropping system was designed such that the mass kept its horizontal position during the free fall. The impact occurred at the lowest point of the fall, with the impact force directed only in the horizontal direction.

5. Instrumentation

The tests were instrumented with optical and hard-wired measurements. Analogue signals measured the force in the two post-tensioned rods, the strain in two points of each of the post-tensioned rods, and the acceleration in two points of the dropping mass. One HS camera measured, by 2D DIC, the movement of the dropping mass in the close vicinity of its impact with the wall. Two other HS cameras were used in stereo mode to obtain, through 3D DIC, full displacement field measurements of the face of the wall opposite to the one subjected to the impacts. Moreover, small steel targets covered with white background and black speckle were secured on the upper and lower RC slabs to screen, through 3D DIC, the fixity conditions of the walls.

Figure 5a shows the instrumentation scheme. Two acquisition systems were used: one for the analogue signals, and one for the images recorded by the three HS cameras. The recording of the HS cameras was started manually by a camera triggering system. The triggering signal was used as an input also in the analogue signal acquisition system, to enable the time synchronization between the latter and the image acquisition system. The time synchronization scheme between the images and analogue signals is illustrated in Figure 5b. The analogue signals were started before the triggering system was triggered. In total, 5 s of analogue signals were stored. The images of the three HS cameras were started manually and simultaneously by the triggering system right before the impact of the dropping mass and they stopped automatically when the memory in the cameras was full. Of the images acquired, not all were stored, but only those belonging to the time window of interest for the impact analysis. In total, 10k images (corresponding to 250 ms) were stored for the 2D DIC measurement, and 15k pairs of images (corresponding to 3 s) for the 3D DIC measurement. The time of impact was determined by observation of the 2D DIC measurements and was defined as the ‘time zero’ ($t_{impact} = 0$) for all the measurements.

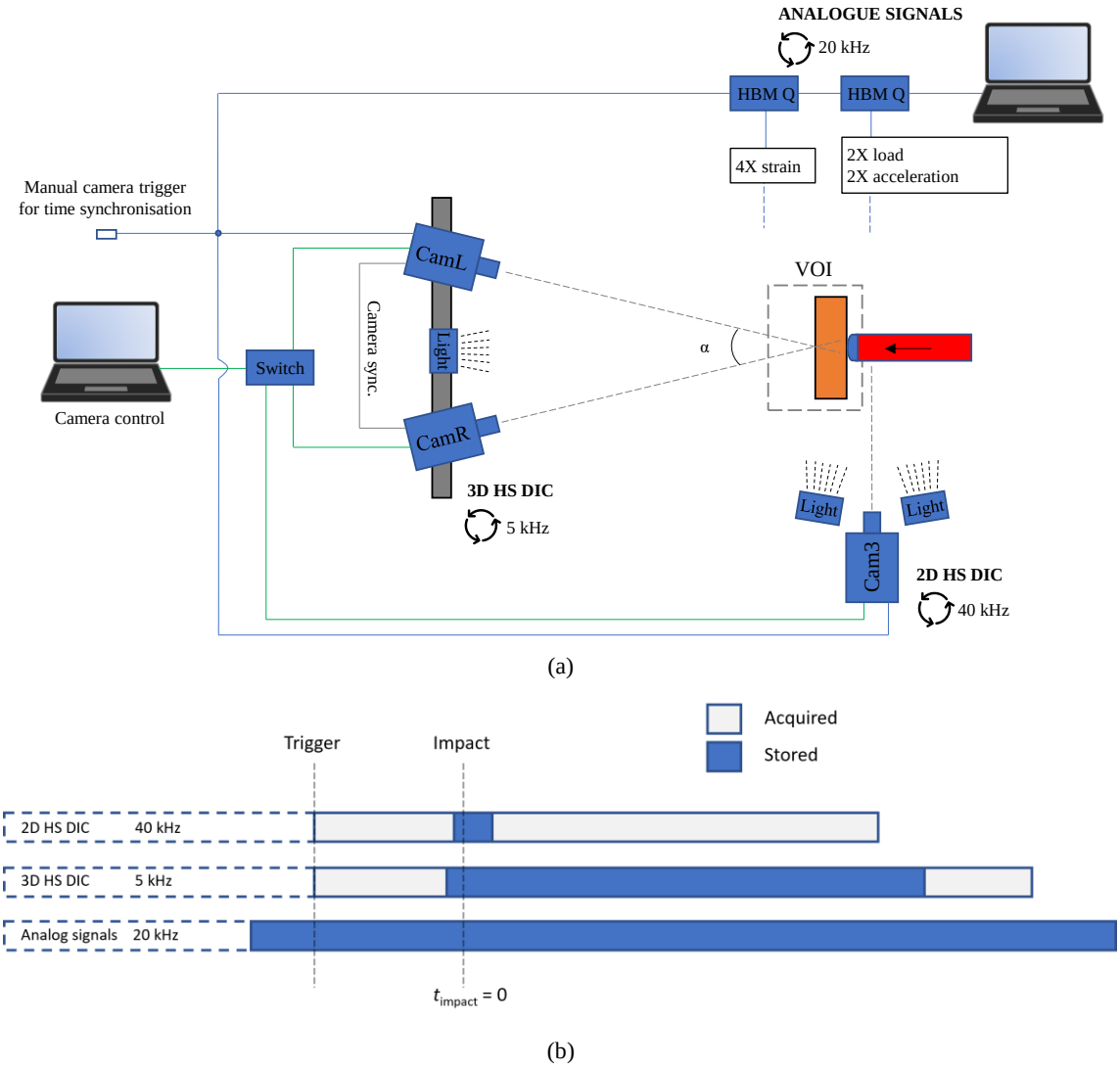

Figure 5 Instrumentation scheme (a) and time synchronization scheme between analogue signals and high-speed (HS) image acquisition for 2D and 3D digital image correlation (DIC) (b).

Analogue signal measurements

Analogue signal acquisition was used to measure the force and strain in the post-tensioned rods, and the acceleration of the dropping mass. An overview of the instrumentation can be seen in Figure 6a.

The axial force in each of the two rods was measured by 200 kN force washer transducers, placed around the rods on top of the transversal loading beam (Figure 6b). A spherical washer was placed between the force transducer and the tightening nut to ensure an even force distribution. The force transducers were used both before the tests, to apply the intended initial axial stress by post-tensioning, and during the tests, to measure the variation in the axial force during the impact (see section 6).

In addition to direct force measurements, the axial strain of the rods was measured by four strain gauges, two for each rod, positioned at the rod mid-height (Figure 6c). Before testing, the rods were gently machined to remove the threads in order to get smooth surfaces where to glue the strain gauges on. The strain measures were then used to derive the axial force in the rods, to be compared with the one measured by the force transducers.

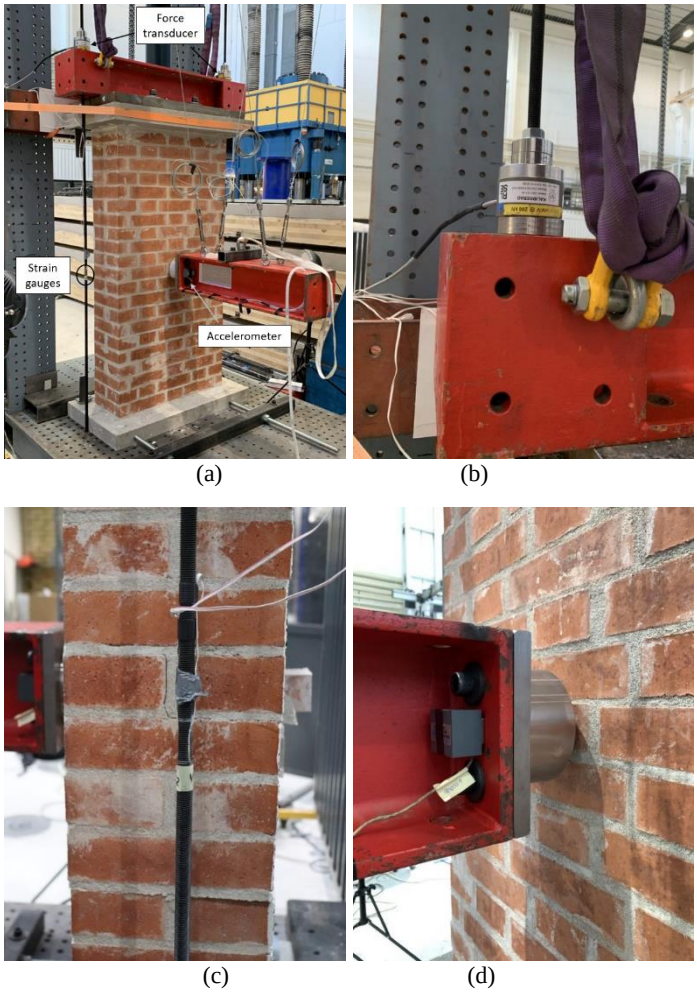

Figure 6 Overview of analogue signal instrumentation (a) and details on the arrangement of the force transducers (b), strain gauges (c), and left-hand side accelerometer (d).

Two accelerometers were positioned at the backside of the beam end flange, one at each side of the beam web (Figure 6d). The accelerometers were attached to the metallic surface of the beam by beeswax to get a good transmission and hold in position by magnetic holders. The acceleration of the dropping mass was calculated as the average value of two accelerometers. The acceleration was then used to derive the impact force.

The analogue signals were acquired to a laptop computer by a data acquisition system consisting of HBM Catman software and HBM QuantumX measuring modules MX840 (force transducers and accelerometers) and MX1615 (strain gauges), with a sampling rate of 20 kHz.

2D high-speed DIC measurements

The movement of the dropping mass was monitored using the 2D DIC technique with a Photron FASTCAM SAZ HS camera to determine its displacement, velocity and acceleration.

The camera was equipped with a 70-200 mm Nikon lens, with the focal length set at 200 mm and the aperture at *f*/4 during the test. The camera was placed at a perpendicular distance of about 1.9 m from the surface of the hemispherical bulb (Figure 7a). A camera resolution of 1024 × 400 pixels and an image acquisition rate of 40 kHz were used, corresponding to a time resolution of 0.025 ms. The camera configuration allowed for a field of view of approximately 223 × 87 mm^2, covering the bulb during the impact. The image spatial resolution and the corresponding field of view was determined by a reference scale. The speckle pattern was printed on self-adhesive paper

that was attached to the cylindrical part of the bulb. To obtain high contrast levels of the pattern, the bulb was illuminated by two high-power led lamps.

The images were analysed by the DIC technique using the proprietary software package GOM Correlate. For each test, a sequence of 2500 images at the occasion of impact were selected for evaluation, corresponding to a time sequence of 62.5 ms. The dimensions of each subset were 30 × 30 pixels and the subset step was 10 pixels, which corresponds to a subset size and data point spacing of approximately 6.5 mm and 2.2 mm, respectively. The displacement resolution was approximately 0.002 mm for both the x- and y-displacement components, determined as the standard deviation between static images of the pattern before loading. To minimize the measuring noise, the displacement, velocity and acceleration were determined as average values of a surface component including approximately 400 data points (Figure 7b).

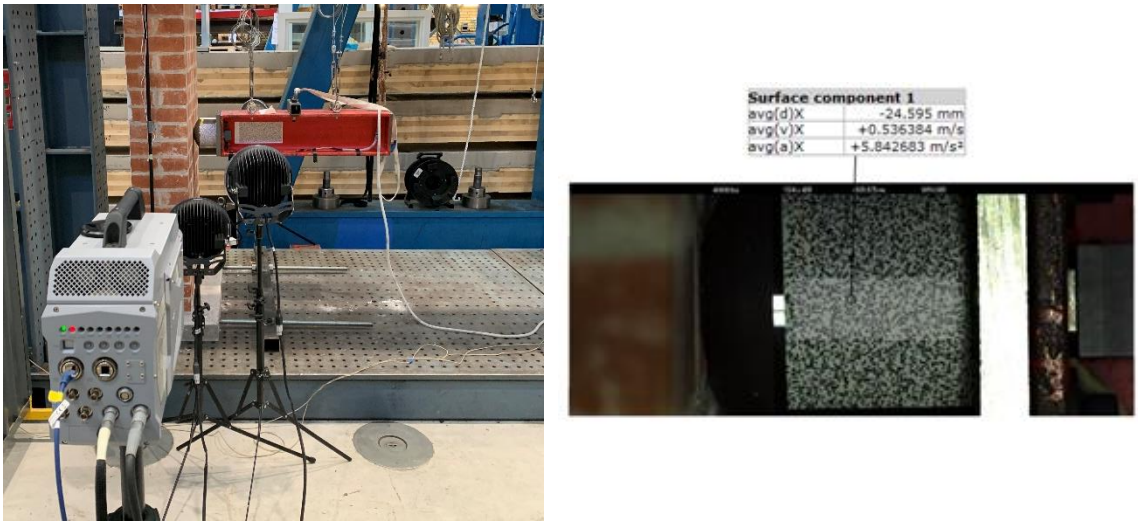

(a) (b)

Figure 7 2D high-speed DIC measurements: View of the setup (a); image from the DIC evaluation (b).

3D high-speed DIC measurements

To analyse the dynamic structural response of the masonry walls, 3D DIC measurements based on a stereoscopic camera set-up with two HS cameras were employed. The measurements were used to study, e.g., the crack development, wall uplift, out-of-plane deformations.

Two Photron Mini AX100 cameras were mounted on a rigid aluminium profile with a relative distance of 1.7 m and angle of 24°. The camera set-up was positioned at distance of approximately 4 m from the surface of the walls. On the cameras were mounted 50 mm fixed Nikon lenses and the aperture was set to *f*/4. An image resolution of 1024 × 720 pixels and an acquisition rate of 5 kHz were used, which corresponds to a time resolution of approximately 0.2 ms. The cameras were synchronized in time by connecting them with a synchronization cable and using a master-slave mode. Before testing, the system configuration was calibrated for a measuring volume of approximately 1565 × 1120 × 1120 mm^3 (x, y, z), covering slightly more than the face of the wall. The speckle pattern used for the subset correlations was achieved by first applying white retro reflective paint as background and then black stains using a rough plastic brush. To obtain high contrast levels, during the tests the walls were illuminated by a high-power white LED light panel.

Figure 8 3D high-speed DIC measurements: View of the set-up.

For each test, 1000 pairs of images (200 ms) were imported and analysed in GOM Correlate. To keep track of the cumulated damage, one image was imported before the first impact of each wall (W9-1, W10-1 and W11-1) and used as reference image in the evaluation of the following impacts. By doing so, deformations, cracks, etc., were related to the undamaged state of the wall prior to testing. The dimensions of each subset were 15 ×15 pixels and the subset step was 10 pixels. For the system configuration employed, this corresponds to a subset size and a data point spacing of approximately 23.3 mm and 15.5 mm, respectively, at the surface of the wall. The displacement resolution was determined to approximately 0.015 mm for both the x- and y-displacement components and approximately 0.050 mm for z-component, determined as the standard deviation between static images of the pattern before loading.

6. Test results

We show here the results of all the impact tests conducted as part of the experimental campaign.

W9-1

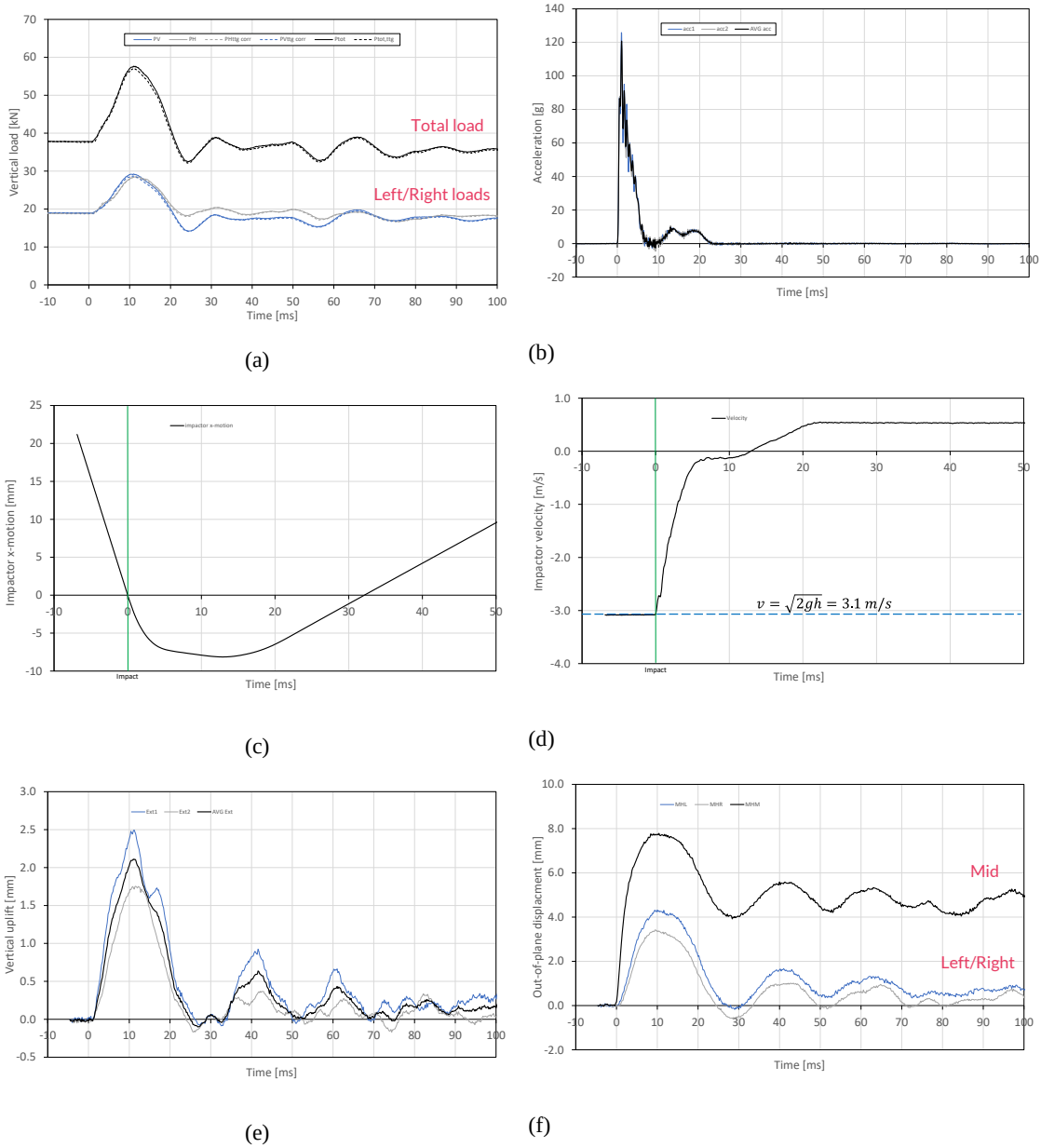

Figure 9 Test results – Wall W9-1: (a) Axial load; (b) Acceleration of the dropping mass; (c) displacement of the dropping mass; (d) velocity of the dropping mass; (e) wall uplift; (f) out-of-plane wall deflection.

W9-2

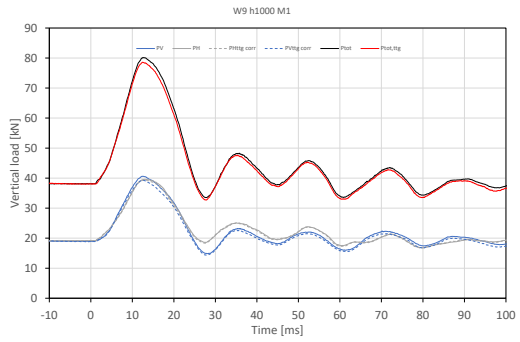

(a)

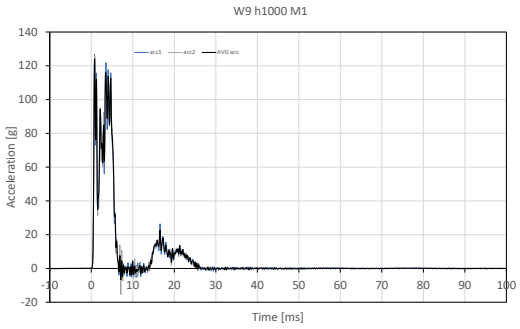

(b)

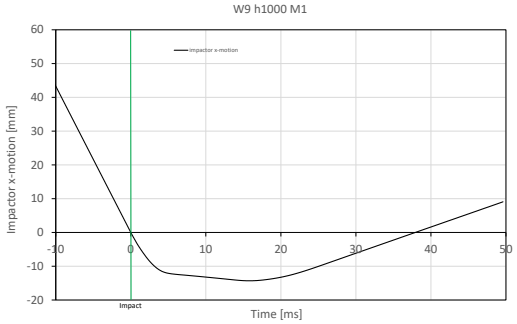

(c)

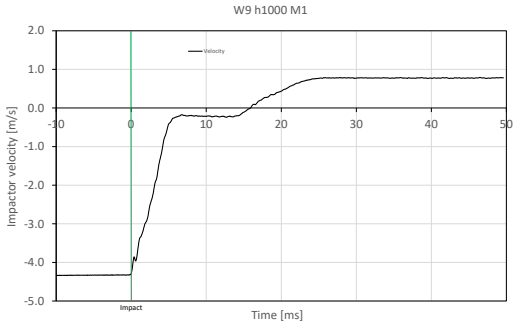

(d)

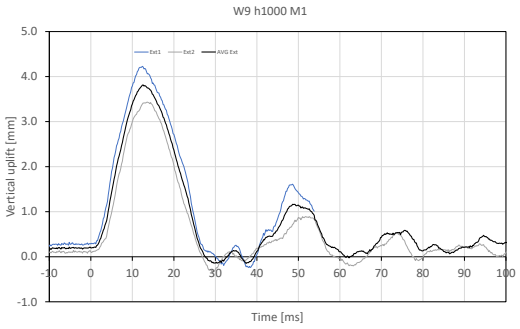

(e)

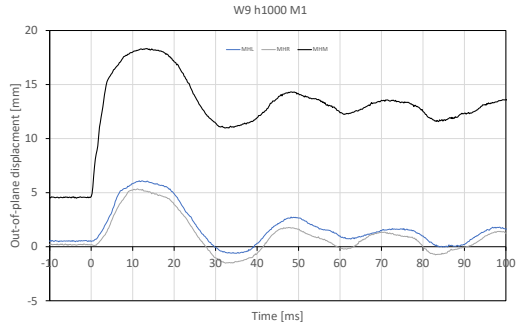

(f)

Figure 10 Test results – Wall W9-2: (a) Axial load; (b) Acceleration of the dropping mass; (c) displacement of the dropping mass; (d) velocity of the dropping mass; (e) wall uplift; (f) out-of-plane wall deflection.

W9-3

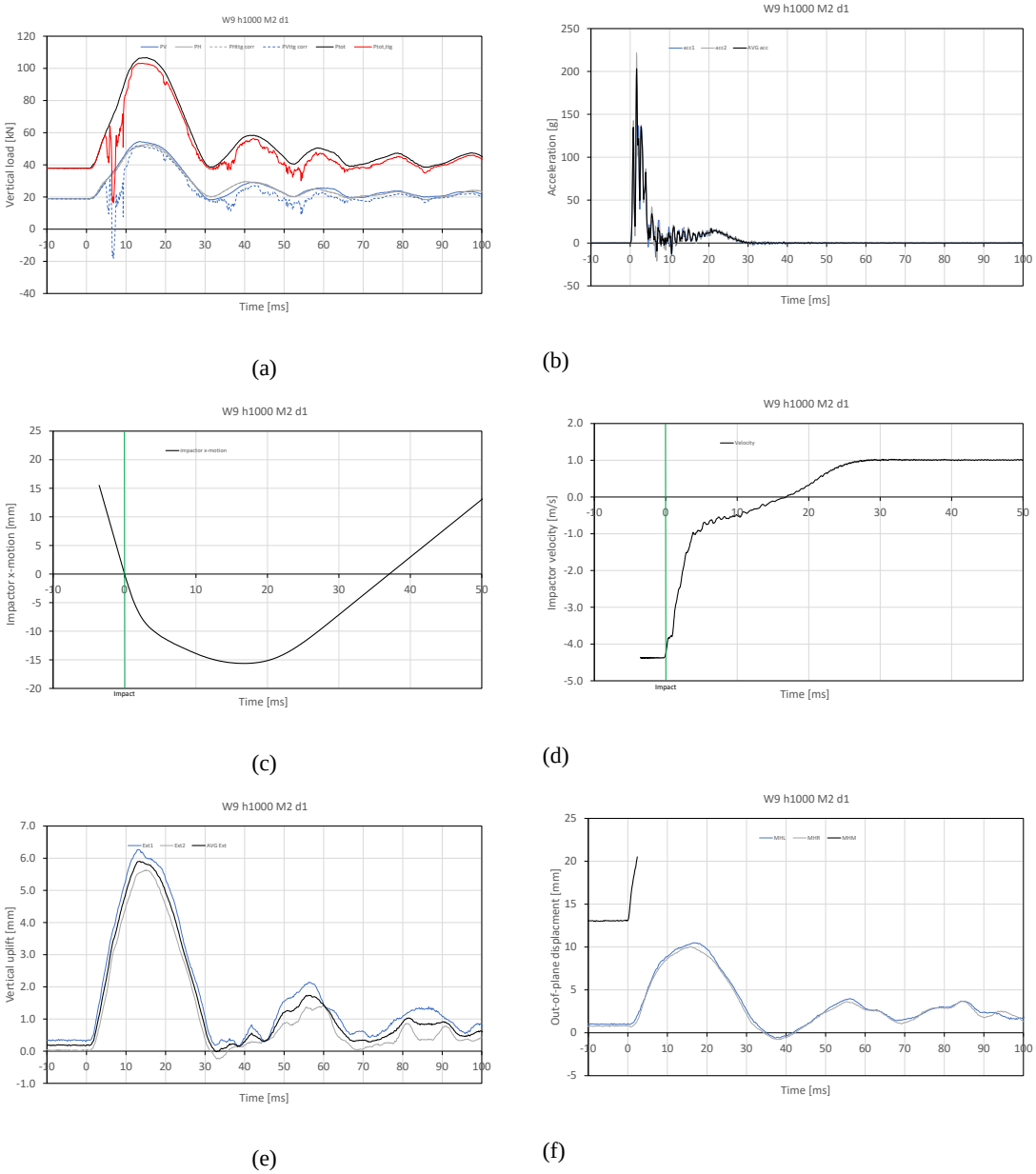

Figure 11 Test results – Wall W9-3: (a) Axial load; (b) Acceleration of the dropping mass; (c) displacement of the dropping mass; (d) velocity of the dropping mass; (e) wall uplift; (f) out-of-plane wall deflection.

W9-4

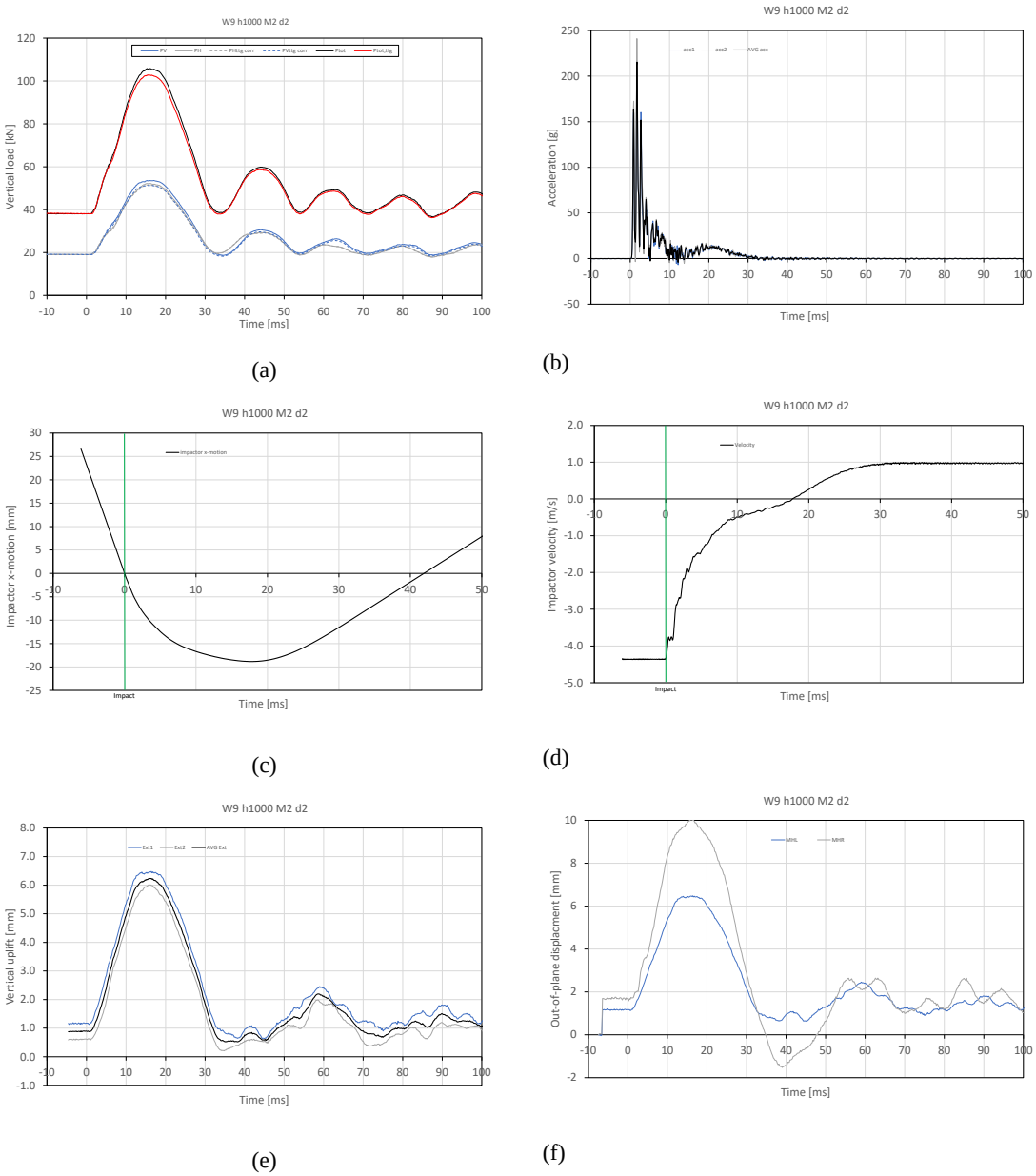

Figure 12 Test results – Wall W9-4: (a) Axial load; (b) Acceleration of the dropping mass; (c) displacement of the dropping mass; (d) velocity of the dropping mass; (e) wall uplift; (f) out-of-plane wall deflection.

W9-5

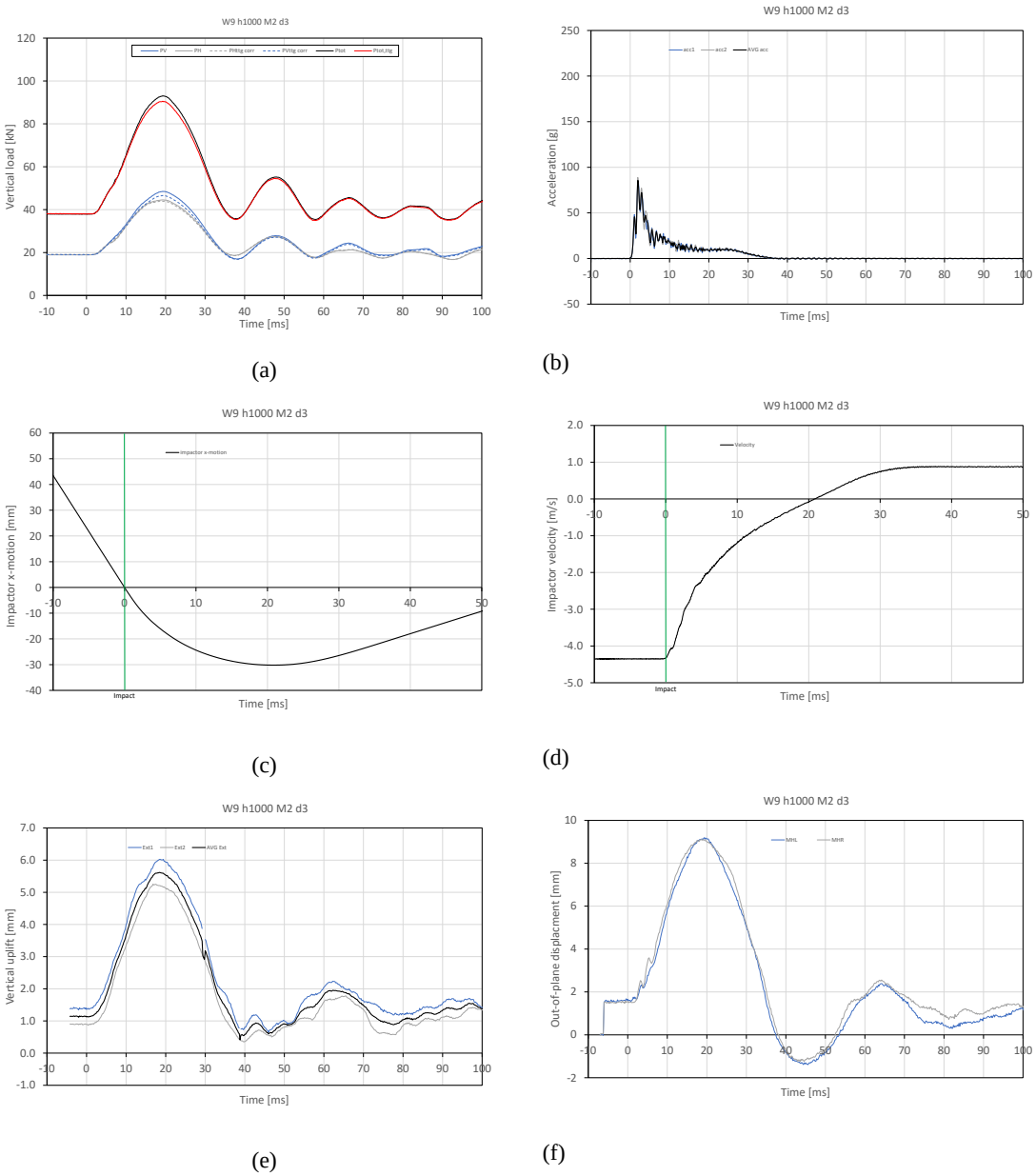

Figure 13 Test results – Wall W9-5: (a) Axial load; (b) Acceleration of the dropping mass; (c) Displacement of the dropping mass; (d) Velocity of the dropping mass; (e) Wall uplift; (f) Out-of-plane wall deflection.

W10-1

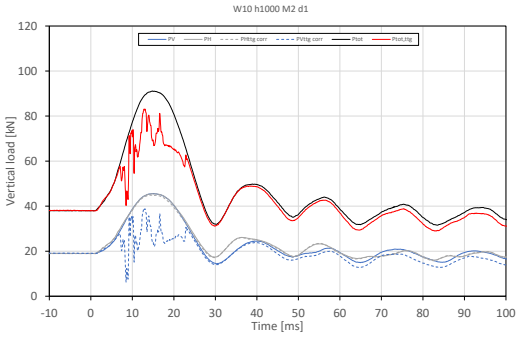

(a)

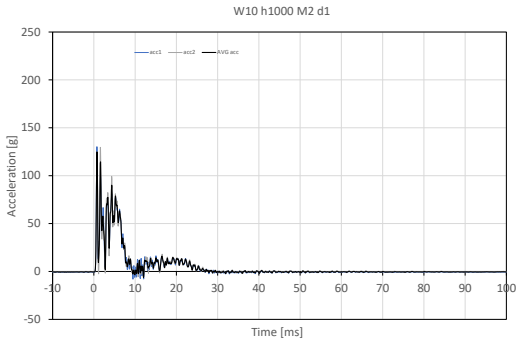

(b)

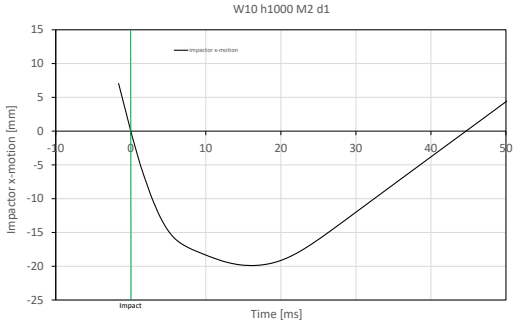

(c)

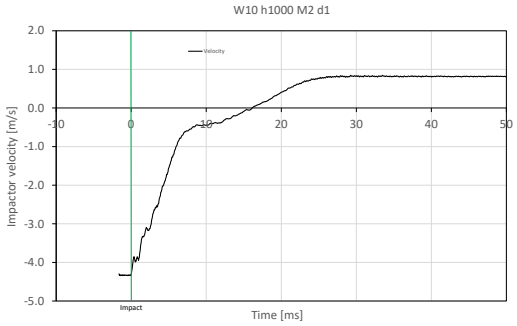

(d)

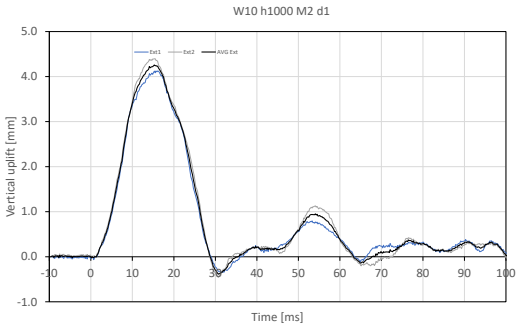

(e)

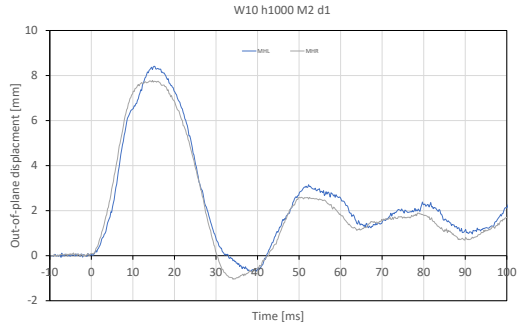

(f)

Figure 14 Test results – Wall W10-1: (a) Axial load; (b) Acceleration of the dropping mass; (c) Displacement of the dropping mass; (d) Velocity of the dropping mass; (e) Wall uplift; (f) Out-of-plane wall deflection.

W10-2

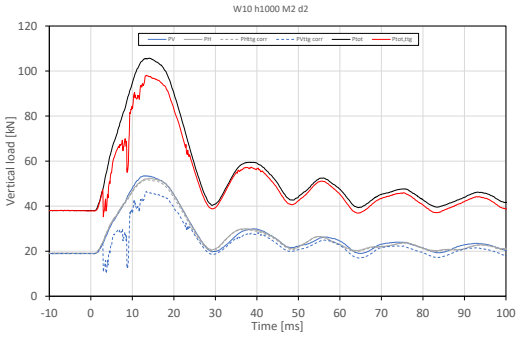

(a)

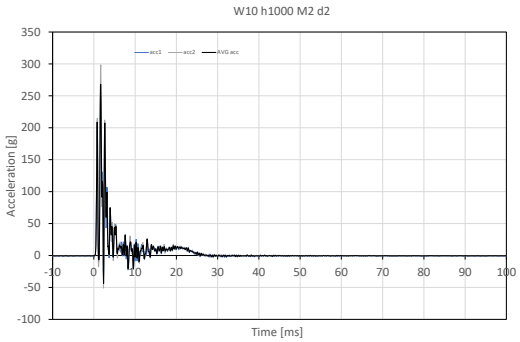

(b)

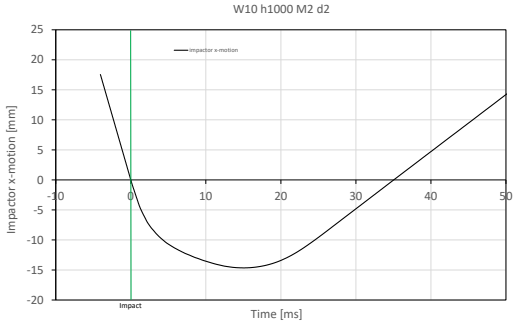

(c)

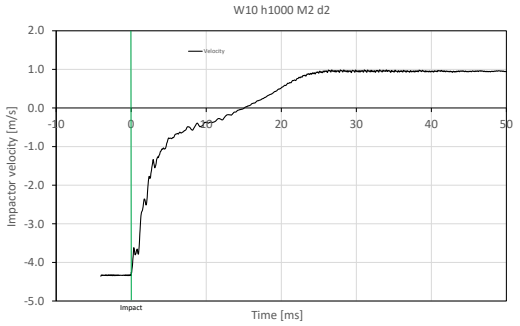

(d)

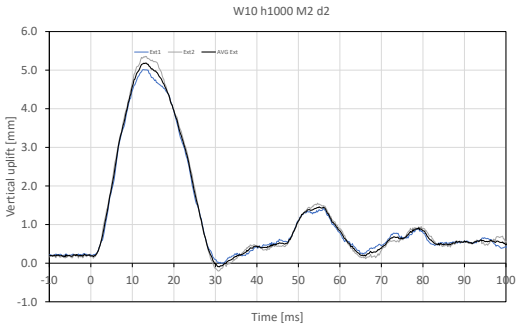

(e)

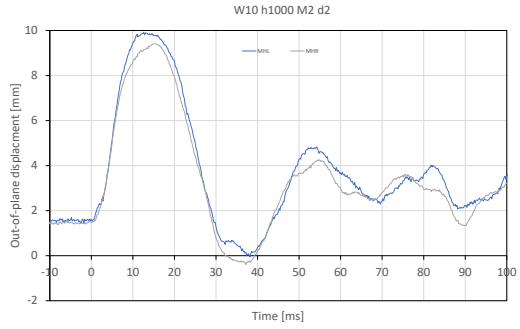

(f)

Figure 15 Test results – Wall W10-2: (a) Axial load; (b) Acceleration of the dropping mass; (c) Displacement of the dropping mass; (d) Velocity of the dropping mass; (e) Wall uplift; (f) Out-of-plane wall deflection.

W10-3

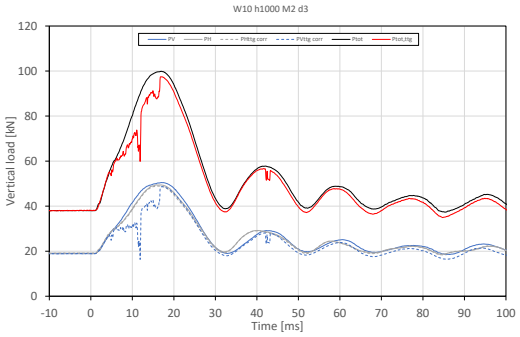

(a)

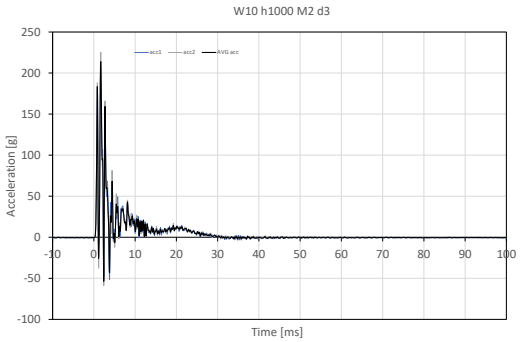

(b)

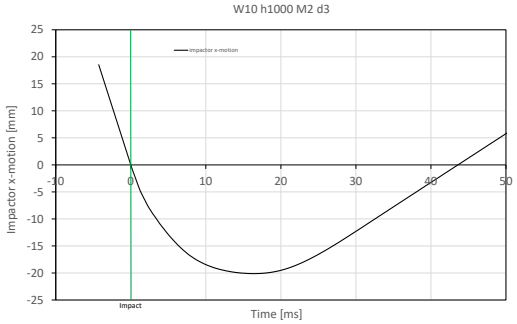

(c)

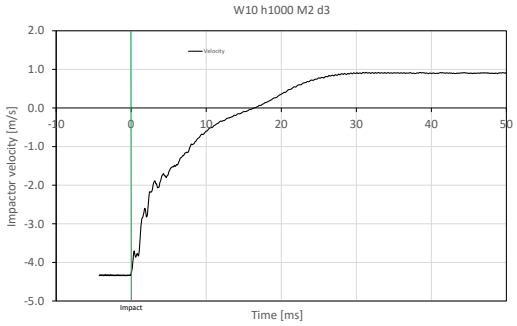

(d)

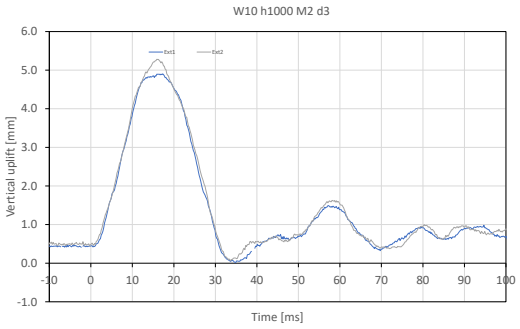

(e)

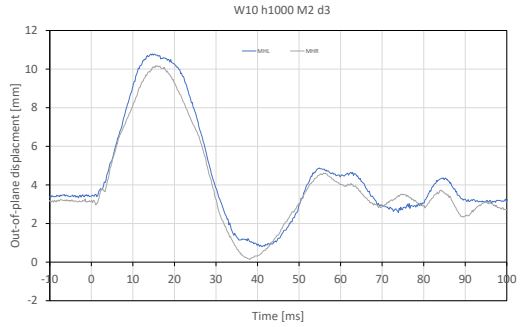

(f)

Figure 16 Test results – Wall W10-3: (a) Axial load; (b) Acceleration of the dropping mass; (c) Displacement of the dropping mass; (d) Velocity of the dropping mass; (e) Wall uplift; (f) Out-of-plane wall deflection.

W10-4

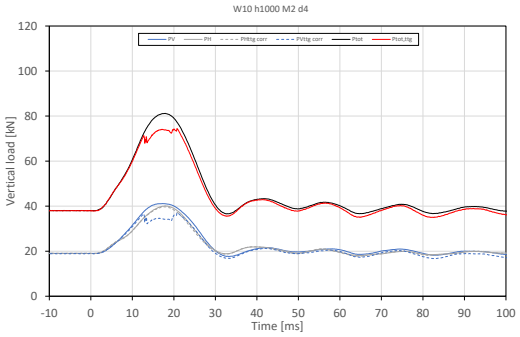

(a)

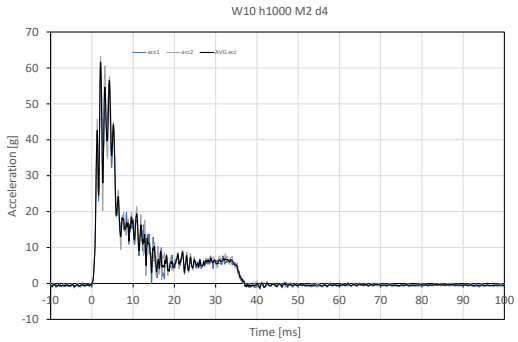

(b)

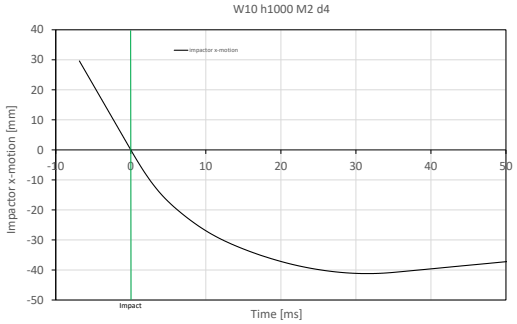

(c)

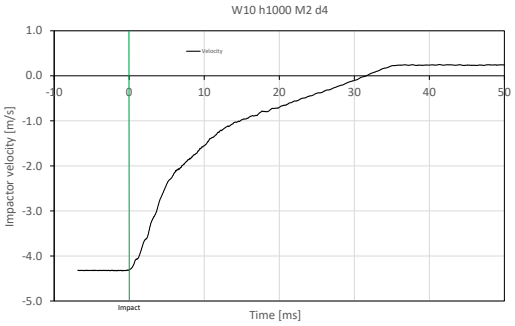

(d)

No results from 3D DIC

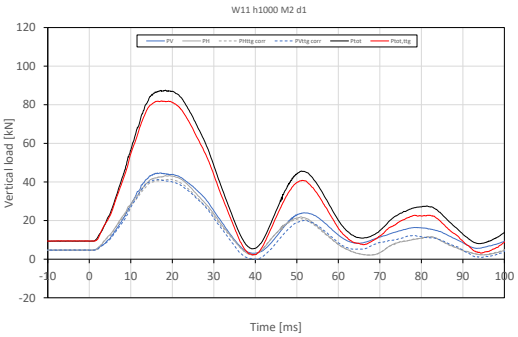

(e)

(f)

Figure 17 Test results – Wall W10-4: (a) Axial load; (b) Acceleration of the dropping mass; (c) Displacement of the dropping mass; (d) Velocity of the dropping mass; (e) Wall uplift; (f) Out-of-plane wall deflection.

W11-1

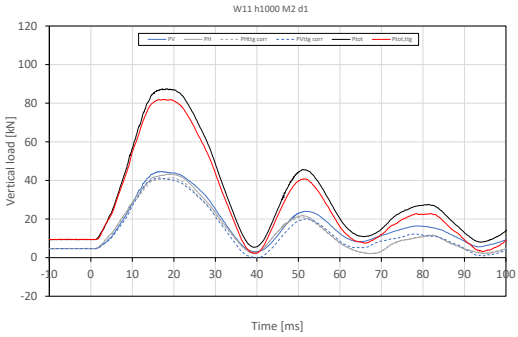

(a)

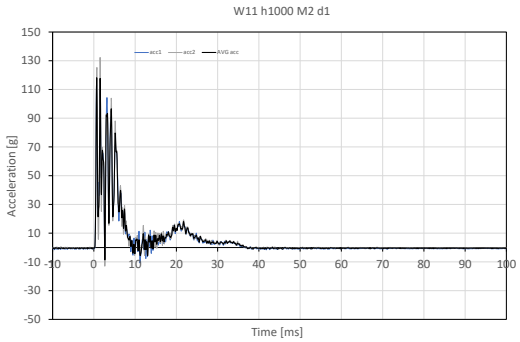

(b)

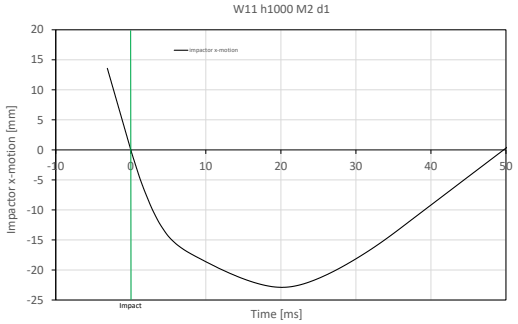

(c)

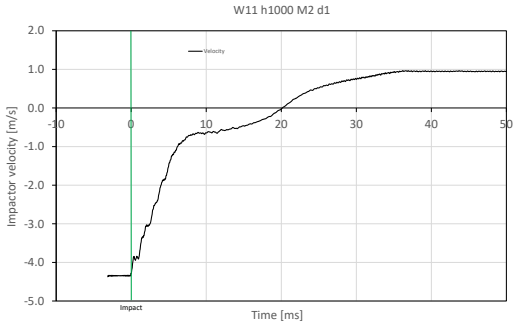

(d)

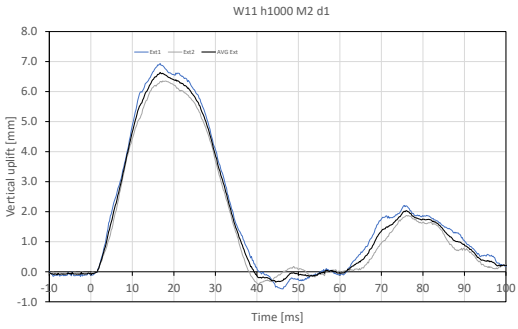

(e)

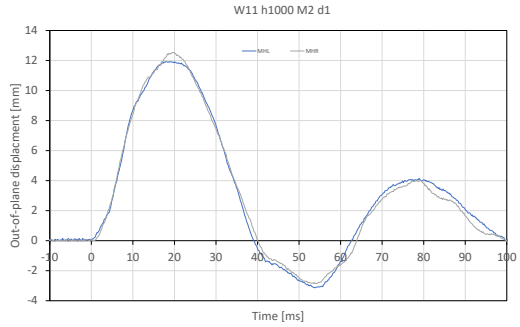

(f)

Figure 18 Test results – Wall W11-1: (a) Axial load; (b) Acceleration of the dropping mass; (c) Displacement of the dropping mass; (d) Velocity of the dropping mass; (e) Wall uplift; (f) Out-of-plane wall deflection.

W11-2

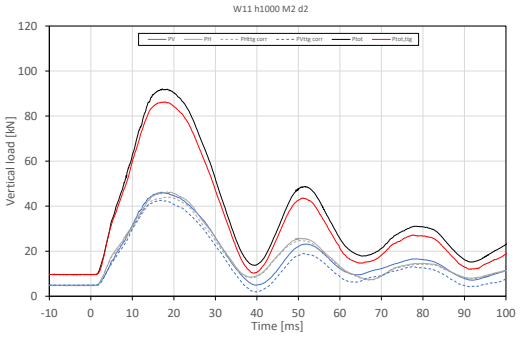

(a)

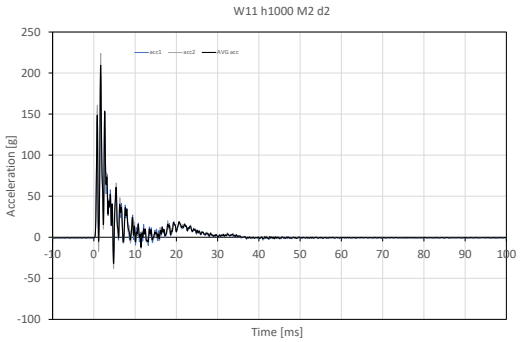

(b)

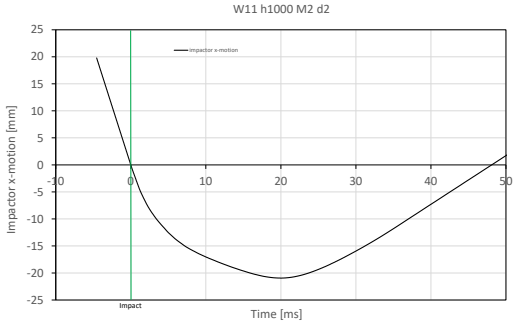

(c)

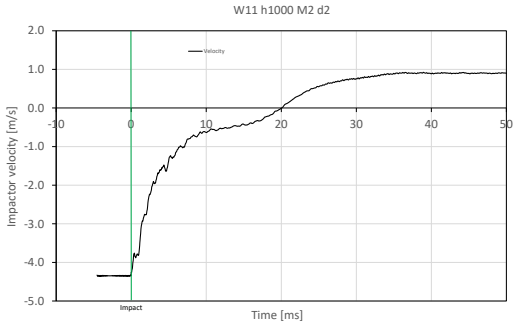

(d)

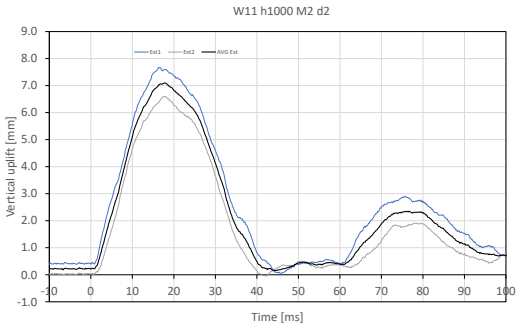

(e)

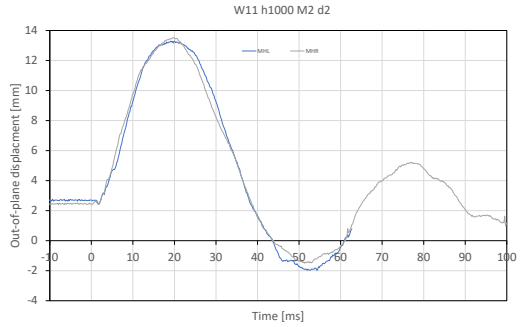

(f)

Figure 19 Test results – Wall W11-2: (a) Axial load; (b) Acceleration of the dropping mass; (c) Displacement of the dropping mass; (d) Velocity of the dropping mass; (e) Wall uplift; (f) Out-of-plane wall deflection.

W11-3

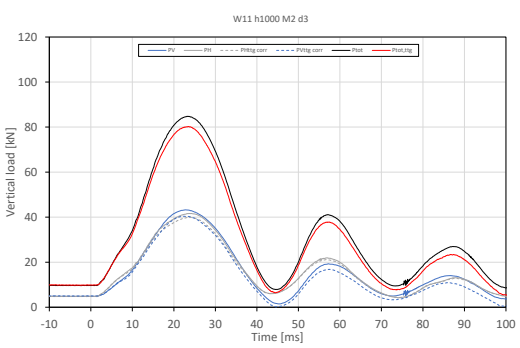

(a)

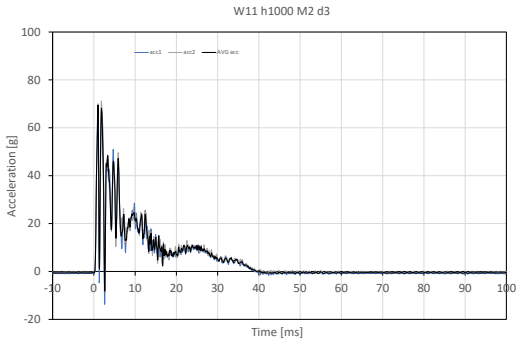

(b)

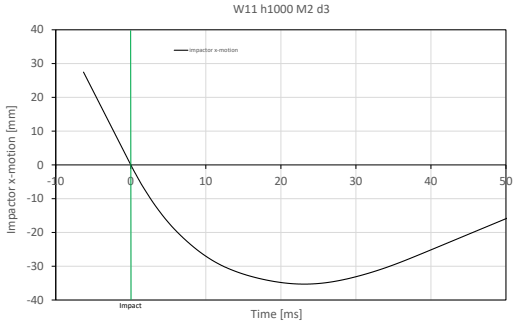

(c)

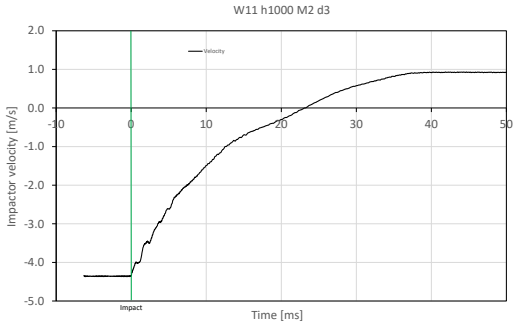

(d)

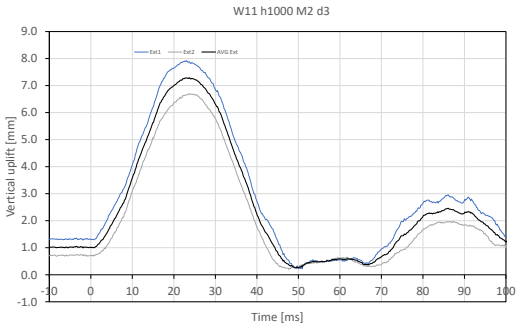

(e)

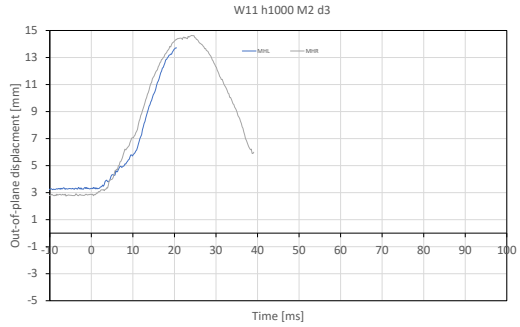

(f)

Figure 20 Test results – Wall W11-3: (a) Axial load; (b) Acceleration of the dropping mass; (c) Displacement of the dropping mass; (d) Velocity of the dropping mass; (e) Wall uplift; (f) Out-of-plane wall deflection.

7. Discussion and outlooks

The study yielded two major contributions:

- The study of the response of brick URM, and the evidence of failure, crack initiation and strain wave propagation within the walls, under different impact conditions.
- The development of an integrated experimental methodology for optical measurements, namely HS-DIC, to be used on URM walls subjected to impacts, and more generally blasts and high strain rate phenomena.

For now, the postprocessing of the results was limited to the analysis of the impact of the dropping mass on the walls. Forthcoming studies will focus on the optical measurements to extend the observations on the wall response: propagation of cracking, cumulation of damage, wall deflection.

References

Acikgoz, S., DeJong, M.J., Soga, K., 2018. Sensing dynamic displacements in masonry rail bridges using 2D digital image correlation. Structural Control and Health Monitoring 25, 1–24. https://doi.org/10.1002/stc.2187

Bolhassani, M., Hamid, A.A., Rajaram, S., Vanniamparambil, P.A., Bartoli, I., Kontsos, A., 2017. Failure analysis and damage detection of partially grouted masonry walls by enhancing deformation measurement using DIC. Engineering Structures 134, 262–275. https://doi.org/10.1016/j.engstruct.2016.12.019

Calderini, C., Degli Abbati, S., Cotič, P., Krzan, M., Bosiljkov, V., 2015. In-plane shear tests on masonry panels with plaster: correlation of structural damage and damage on artistic assets. Bulletin of Earthquake Engineering 13, 237–256. https://doi.org/10.1007/s10518-014-9632-y

Cinar, A.F., Barhli, S.M., Hollis, D., Flansbjer, M., Tomlinson, R.A., Marrow, T.J., Mostafavi, M., 2017. An autonomous surface discontinuity detection and quantification method by digital image correlation and phase congruency. Optics and Lasers in Engineering 96, 94–106. https://doi.org/10.1016/j.optlaseng.2017.04.010

Dhanasekar, M., Prasad, P., Dorji, J., Zahra, T., 2019. Serviceability Assessment of Masonry Arch Bridges Using Digital Image Correlation. Journal of Bridge Engineering 24, 1–16. https://doi.org/10.1061/(ASCE)BE.1943-5592.0001341

EN 772-1, 2015. Methods of test for masonry units - Part 1: Determination of compressive strength.

EN 1015-11, 2019. Methods of test for mortar for masonry - Part 11: Determination of flexural and compressive strength of hardened mortar.

EN 1052-1, 1992. Methods of test for masonry - Part 1: Determination of compressive strength.

EN 1052-5, 2005. Methods of test for masonry - Part 5 : Determination of bond strength by the bond wrench method.

Flansbjer, M., Williams Portal, N., Vennetti, D., Mueller, U., 2018. Composite Behaviour of Textile Reinforced Reactive Powder Concrete Sandwich Façade Elements. International Journal of Concrete Structures and Materials 12. https://doi.org/10.1186/s40069-018-0301-4

Ghorbani, R., Matta, F., Sutton, M.A., 2015. Full-Field Deformation Measurement and Crack Mapping on Confined Masonry Walls Using Digital Image Correlation. Experimental Mechanics 55, 227–243. https://doi.org/10.1007/s11340-014-9906-y

Gilbert, M., Hobbs, B., Molyneaux, T.C.K., 2002. The performance of unreinforced masonry walls subjected to low-velocity impacts: experiments. International Journal of Impact Engineering 27, 231–251. https://doi.org/10.1016/S0734-743X(01)00049-5

Godio, M., Vanin, F., Zhang, S., Beyer, K., 2019. Quasi-static shear-compression tests on stone masonry walls with plaster: Influence of load history and axial load ratio. Engineering Structures 192, 264–278. https://doi.org/10.1016/j.engstruct.2019.04.041

Godio, M., Williams Portal, N., Flansbjer, M., Magnusson, J., Byggnevi, M., 2021. Experimental and numerical approaches to investigate the out-of-plane response of unreinforced masonry walls subjected to free far-field blasts. Engineering Structures 239, 112328. https://doi.org/10.1016/j.engstruct.2021.112328

Guerrero, N., Martínez, M., Picón, R., Marante, M.E., Hild, F., Roux, S., Flórez-López, J., 2014. Experimental analysis of masonry infilled frames using digital image correlation. Materials and Structures/Materiaux et Constructions 47, 873–884. https://doi.org/10.1617/s11527-013-0099-0

Hao, H., Tarasov, B.G., 2008. Experimental Study of Dynamic Material Properties of Clay Brick and Mortar at Different Strain Rates. Australian Journal of Structural Engineering 8, 117–132. https://doi.org/10.1080/13287982.2008.11464992

Jin, H., Sciammarella, C., Yoshida, S., Lamberti, L., 2016. Advancement of Optical Methods in Experimental Mechanics, Volume 3. https://doi.org/10.1007/978-3-319-00768-7

Masi, F., Stefanou, I., Vannucci, P., 2018. A study on the effects of an explosion in the Pantheon of Rome. Engineering Structures 164, 259–273. https://doi.org/10.1016/j.engstruct.2018.02.082

Masi, F., Stefanou, I., Vannucci, P., Maffi-Berthier, V., 2019. Rocking response of inverted pendulum structures under blast loading. International Journal of Mechanical Sciences 157–158, 833–848. https://doi.org/10.1016/j.ijmecsci.2019.05.024

Michaloudis, G., Gebbeken, N., 2019. Modeling masonry walls under far-field and contact detonations. International Journal of Impact Engineering 123, 84–97. https://doi.org/10.1016/j.ijimpeng.2018.09.019

Mojsilović, N., Salmanpour, A.H., 2016. Masonry walls subjected to in-plane cyclic loading: application of digital image correlation for deformation field measurement. International Journal of Masonry Research and Innovation 1, 165. https://doi.org/10.1504/ijmri.2016.077473

Nabouch, R. El, Bui, Q.B., Plé, O., Perrotin, P., 2019. Rammed earth under horizontal loadings: Proposition of limit states. Construction and Building Materials 220, 238–244. https://doi.org/10.1016/j.conbuildmat.2019.06.020

Nghiem, H.L., Al Heib, M., Emeriault, F., 2015. Method based on digital image correlation for damage assessment in masonry structures. Engineering Structures 86, 1–15. https://doi.org/10.1016/j.engstruct.2014.12.021

Rezaie, A., Achanta, R., Godio, M., Beyer, K., 2020a. Comparison of crack segmentation using digital image correlation measurements and deep learning. Construction and Building Materials 261, 120474. https://doi.org/10.1016/j.conbuildmat.2020.120474

Rezaie, A., Godio, M., Achanta, R., Beyer, K., 2020b. Machine-learning for damage assessment of rubble stone masonry piers based on crack patterns. Automation in Construction.

Rezaie, A., Godio, M., Beyer, K., 2021. Investigating the cracking of plastered stone masonry walls under shear–compression loading. Construction and Building Materials 306, 124831. https://doi.org/10.1016/j.conbuildmat.2021.124831

Rezaie, A., Godio, M., Beyer, K., 2019. Experimental Investigation of Strength, Stiffness and Drift Capacity of Rubble Stone Masonry Walls. under review (submitted).

Salmanpour, A.H., Mojsilović, N., Schwartz, J., 2015. Displacement capacity of contemporary unreinforced masonry walls: An experimental study. Engineering Structures 89, 1–16. https://doi.org/10.1016/j.engstruct.2015.01.052

Shetty, N., Livitsanos, G., van Roy, N., Aggelis, D.G., van Hemelrijck, D., Wevers, M., Verstrynge, E., 2019. Quantification of progressive structural integrity loss in masonry with Acoustic Emission-based damage classification. Construction and Building Materials 194, 192–204. https://doi.org/10.1016/j.conbuildmat.2018.10.215

Sieffert, Y., Vieux-Champagne, F., Grange, S., Garnier, P., Duccini, J.C., Daudeville, L., 2016. Full-field measurement with a digital image correlation analysis of a shake table test on a timber-framed structure filled with stones and earth. Engineering Structures 123, 451–472. https://doi.org/10.1016/j.engstruct.2016.06.009

Sielicki, P.W., Łodygowski, T., 2019. Masonry wall behaviour under explosive loading. Engineering Failure Analysis 104, 274–291. https://doi.org/10.1016/j.engfailanal.2019.05.030

Skellefteå Museum, 2019. Hålla hus - Tegel- och betongstommar [WWW Document]. URL http://hallahus.se/renovera/stommen/tegel-och-betongstommar/murtegel/ (accessed 12.2.19).

Sutton, M.A., Orteu, J.-J., Schreier, H., 2009. Image correlation for shape, motion and deformation measurements. Springer US, Boston, MA. https://doi.org/10.1007/978-0-387-78747-3

Williams Portal, N., Flansbjer, M., Honfi, D., 2019. Testing of self-supporting laminated glass balustrades.

Williams Portal, N., Godio, M., Flansbjer, M., 2020. Blast capacity of masonry walls – A preliminary study.

Williams Portal, N., Godio, M., Flansbjer, M., Magnusson, J., Byggnevi, M., 2022. Out-of-plane pushover tests on single- and double-wythe brick masonry walls instrumented with optical measurements: influence of local deformations and arching action on wall capacity. Under preparation.